Experimental Neurology 318 (2019) 232–243

Contents lists available at ScienceDirect

Experimental Neurology

journal homepage: www.elsevier.com/locate/yexnr

Research Paper

Visual discrimination impairment after experimental stroke is associated with disturbances in the polarization of the astrocytic aquaporin-4 and increased accumulation of neurotoxic proteins

Sonia Sanchez-Bezanilla[a,b], Clifford TeBay[a], Michael Nilsson[a,b,c,d,e], Frederick R. Walker[a,b,c,d], Lin Kooi Ong[a,b,c,*]

[a] School of Biomedical Sciences and Pharmacy and Priority Research Centre for Stroke and Brain Injury, University of Newcastle, Callaghan, NSW, Australia
[b] Hunter Medical Research Institute, New Lambton, Heights, NSW, Australia
[c] NHMRC Centre of Research Excellence Stroke Rehabilitation and Brain Recovery, Heidelberg, VIC, Australia
[d] Centre for Rehab Innovations, University of Newcastle, Callaghan, NSW, Australia
[e] LKC School of Medicine, Nanyang Technological University, Singapore

ARTICLE INFO

Keywords:
α-Synuclein
Amyloid-β
Aquaporin-4
Cognitive impairment
Stroke

ABSTRACT

Numerous clinical studies have documented the high incidence of cognitive impairment after stroke. However, there is only limited knowledge about the underlying mechanisms. Interestingly, there is emerging evidence suggesting that cognitive function after stroke may be affected due to reduced waste clearance and subsequent accumulation of neurotoxic proteins. To further explore this potential association, we utilised a model of experimental stroke in mice. Specifically, a photothrombotic vascular occlusion targeting motor and sensory parts of the cerebral cortex was induced in young adult mice, and changes in cognition were assessed using a touchscreen platform for pairwise visual discrimination. The results showed that the execution of the visual discrimination task was impaired in mice 10 to 14 days post-stroke compared to sham. Stroke also induced significant neuronal loss within the peri-infarct, thalamus and the CA1 sub-region of the hippocampus. Further, immunohistochemical and protein analyses of the selected brain regions revealed an increased accumulation and aggregation of both amyloid-β and α-synuclein. These alterations were associated with significant disturbances in the aquaporin-4 protein expression and polarization at the astrocytic end-feet. The results suggest a link between the increased accumulation of neurotoxic proteins and the stroke-induced cognitive impairment. Given that the neurotoxic protein accumulation appeared alongside changes in astrocytic aquaporin-4 distribution, we suggest that the function of the waste clearance pathways in the brain post-stroke may represent a therapeutic target to improve brain recovery.

1. Introduction

Stroke is associated with an elevated risk of cognitive impairment and dementia (Kuzma et al., 2018). Clinically, several studies have documented that up to 80% of stroke survivors experience some level of cognitive deficit (Levine et al., 2015). The cognitive domains which are commonly affected in stroke survivors include memory, learning and executive functions (Sun et al., 2014). However, the cellular mechanisms behind these deficits are yet to be determined. Although larger lesions are associated with greater cognitive impairment after stroke, the size and location of the primary infarct do not reliably predict the extent of these deficits (Gottesman and Hillis, 2010; Saczynski et al., 2009). One explanation for the modest association between cognitive impairment and tissue loss is that prior work has not taken into consideration loss of tissue at secondary sites. There is now mounting evidence demonstrating that stroke initiates delayed tissue and neuronal loss in remote regions that are functionally connected to the primary infarction site, a phenomenon increasingly referred to as secondary neurodegeneration (SND) (Baumgartner et al., 2018; Ong et al., 2017a; Wang et al., 2004; Xie et al., 2011).

Abbreviations: SND, secondary neurodegeneration; CSF, cerebrospinal fluid; ISF, recirculation and interstitial fluid; AQP4, aquaporin 4; PAL, paired associate learning; Aβ, amyloid-β; VD, visual discrimination; α-Syn, α-synuclein; DG, dentate gyrus

* Corresponding author at: School of Biomedical Sciences and Pharmacy and the Priority Research Centre for Stroke and Brain Injury, University of Newcastle, Callaghan, NSW, Australia.
E-mail address: lin.ong@uon.edu.au (L.K. Ong).

https://doi.org/10.1016/j.expneurol.2019.05.001
Received 19 February 2019; Received in revised form 3 April 2019; Accepted 6 May 2019
Available online 09 May 2019
0014-4886/

SND has been consistently observed in clinical neuroimaging studies and in pre-clinical studies (Ong et al., 2017a; Zhang et al., 2012b), develops within days and can last for weeks, months and even years after the primary infarction. The key hallmarks of SND include neuronal death, neuroinflammation and increased accumulation of neurotoxic proteins (such as amyloid-β (Aβ)) (Iizuka et al., 1990; Kluge et al., 2018; Makinen et al., 2008; Patience et al., 2015; van Groen et al., 2005). Recently, our research team has reported that the accumulation of Aβ observed within the thalamus (a major site of SND) after stroke is associated with enhancement of soluble Aβ oligomers (Ong et al., 2017b). Previous studies have also shown that these neurotoxic proteins and in particular soluble oligomers are linked to cellular pathology and cognitive decline within the context of neurodegenerative diseases (Lesne et al., 2006; Lesne et al., 2013). Critically, these neurotoxic proteins continue to build up overtime after stroke (Aho et al., 2006; Liu et al., 2015a; Sahathevan et al., 2016) and several studies suggest that this might be due to a failure in their clearance (Arbel-Ornath et al., 2013; Garcia-Alloza et al., 2011). It is well documented that paravascular cerebrospinal fluid (CSF) recirculation and interstitial fluid (ISF) solute clearance is dependent upon the astroglial aquaporin-4 (AQP4) water channel (Iliff et al., 2012; Peng et al., 2016; Wang et al., 2017), and disturbances in this water channel has been previously linked with impaired clearance in different neurological conditions (Iliff et al., 2014; Ren et al., 2013; Wang et al., 2012).

Our group has recently identified that stroke, induced through photothrombotic vascular occlusion of the somatosensory and motor cortex, produces significant impairment of learning and memory using a touchscreen based assessment of paired associate learning (PAL) (Ong et al., 2018; Zhao et al., 2018). We further identified that the impaired performance was associated with significant accumulation of amyloid-β (Aβ) within the peri-infarct territories (Zhao et al., 2018). In this study, we aimed to determine whether the impairments that we previously observed in PAL task performance after a cortical stroke are generalizable to other cognitive domains. Specifically, we examined whether cognitive impairment are also generalised to other forms of visual-spatial memory, such as that assessed using the visual discrimination (VD) task (Horner et al., 2013). Further, we also intended to explore the molecular and cellular mechanisms behind these deficits. We investigated the accumulation and aggregation of not only Aβ but also α-synuclein (α-Syn), a second protein extensively linked to neurodegeneration (Kim et al., 2016; Stoica et al., 2012). We considered the accumulation of these proteins not only in the peri-infarct territory but also in SND sites, such as the thalamus and hippocampus. Finally, we investigated the changes in the polarization of AQP4 in each of these regions.

Our primary hypothesis was that stroke would reduce the ability of mice to discriminate between two different stimuli. Secondly, we hypothesised that these deficits might be due to increased accumulation of Aβ and α-Syn in the brain. Finally, we proposed that disturbances in the polarization of AQP4 might play an important role in the accumulation of neurotoxic proteins and loss of neuronal cells, leading to cognitive impairment.

2. Materials and methods

The data that supports the findings for this study are available from the corresponding author on reasonable request. An extended methods section is provided in the Supplementary Material.

2.1. Experimental design

Animal research was undertaken in accordance with the ARRIVE guidelines (Animal Research: Reporting of In Vivo Experiments). All the experimental groups were randomized, and all outcome analyses were performed in a blinded manner. A total of 62 mice (C57BL/6 male, 10 weeks old) were used in this study. Details on animal numbers for each experiment and inclusion/exclusion criteria are included in the supplementary material (Supplementary Fig. 1). The first cohort (sham $n = 10$, stroke $n = 11$) were subjected to a mouse touchscreen platform for VD task using images with a low similarity index (default images; fan and marble). The second cohort (sham $n = 10$, stroke $n = 11$) were subjected to VD task using images with a high similarity index and the brain tissue was used for histology analyses. The third cohort of mice (sham $n = 7$, stroke n = 7) were allocated for western blotting. At day 0, mice were subjected to photothrombotic occlusion or sham surgery. At day 3 post-stroke, mice were subjected to a mouse touchscreen platform for VD task during 10 consecutive days (days 3 to 13). Motor tests were performed one day before stroke/sham surgery and at day 14 before the mice were euthanized. Brains and blood samples were collected at 14 days post-stroke.

2.2. Sample size calculation

Sample size was estimated using G*Power 3.1 software. To determine the sample size required for the first and second cohort, we used preliminary data from the VD task (% correct rate at final session; sham versus stroke), and we obtained an effect size of Cohen's $d = 1.5$. Allowing a type 1 error of 5%, $\alpha = 0.05$ with the power of 80%, $\beta = 0.2$ we calculated a sample size of 9 mice per group. > 9 mice per group would ensure that a stroke effect will be detected. For the third cohort (western blot analyses), we obtained an effect size of $d = 2$ and we calculated a sample size of 6 mice per group.

2.3. Photothrombotic occlusion

Photothrombotic occlusion was performed as previously described (Zhao et al., 2017). This model is recognised to possess a number of advantages, including that is highly reproducible, has low experiment to experiment variance, controllable vascular occlusion size and location, and is widely used and extensively validated (Corbett et al., 2017; Uzdensky, 2018). Briefly, mice were anaesthetized by 2% isoflurane during surgical procedure on a temperature controlled (37 °C ± 1) stereotaxic frame. The skull was exposed by incision of the skin along the midline of the scalp. Rose Bengal (200 µl 10 mg/ml solution in sterile saline, Sigma-Aldrich, USA) was injected intraperitoneally. After 8 min, the skull was illuminated for 15 min by a 4.5 mm diameter cold light source positioned at 2.2 mm left lateral of Bregma 0.0 mm, targeting the left motor and somatosensory cortices. For the sham group, the same surgical procedure was applied except Rose Bengal was replaced with 200 µl of sterile saline (0.9% NaCl, Pfizer, Australia).

2.4. Visual discrimination (VD) task

Mouse touchscreen operant chambers were used in the cognitive testing as described with modifications (Horner et al., 2013), and were conducted in a blinded and randomized manner. Mice were calorie restricted overnight before cognitive testing (allowed access to food after cognitive testing for 5 h, between 12:00–17:00 h). A liquid reward (strawberry milkshake) was provided to motivate the performance of the mice. Mice were introduced to a series of habituation and basic training tasks where they learn to associate a nose poke of the touchscreen and the delivery of a liquid reward. Over 10 days all mice learnt to perform the task with a minimum correct rate of 70%. Following general touchscreen training, mice underwent photothrombotic occlusion surgery. Three days post-surgery, mice commenced the VD task. Briefly, the procedure entailed simultaneous presentation of two stimuli; one was programmed as being correct (S+) and one as being incorrect (S-). Whether the S+ was on the right or left was determined pseudorandomly. When the mouse made a correct choice, S+, a tone was triggered, the food tray was illuminated and the food reward was delivered (a correct trial was recorded). If the mouse touched the incorrect image, S-, there was no reward delivery, no tone, and the house

light was turned on for 5 s and a correction trial was initiated. Correction trials consisted of repeated presentation of the previous trial until a correct response was made and were not counted towards the trial limit or number of correct responses. In each VD session, the testing ended once a mouse successfully completed 30 trials or reached a 60 min time limit, whichever occurred first. All mice completed a total of 10 sessions.

2.5. Paw asymmetry assessment using the cylinder task

Motor function was evaluated by a cylinder test as previously described (Schaar et al., 2010). Briefly, one day before stroke (day −1) and day 14 post-stroke, each mouse was placed in a glass cylinder 9 cm diameter and 15 cm in height, and movements were recorded from both sides for 10 min. Paw placement was determined by a researcher blinded to the experimental condition. The first forelimb to contact the wall during a full rear was recorded as an independent wall placement for that limb. The simultaneous contact of both the left and right forelimbs to the wall during a full rear was considered as one placement for both limbs. A total of 20 touches were scored. A final asymmetry score was calculated as the ratio of non-impaired forelimb movement minus impaired forelimb movement to total forelimb movement.

2.6. Protein extraction and western blotting

The peri-infarct territory (2 mm^2 around infarct core, Bregma +1.0 to −1.0 mm), the thalamus (Bregma −1.2 to −2.2 mm) and the hippocampus (Bregma −1.2 to −2.5 mm) were punched using a 1 mm tissue punch. Samples were sonicated in 300 µl lysis buffer (50 mM TRIS buffer pH 7.4, 1 mM EDTA, 1 mM DTT, 80 µM ammonium molybdate, 1 mM sodium pyrophosphate, 1 mM sodium vanadate, 5 mM b-glycerolphosphate, 1 protease inhibitor cocktail tablet, 1 phosphatase inhibitor cocktail tablet, final concentration) and centrifuged at 14000*g* for 20 min at 4 °C. The supernatant fractions were collected and pellet fractions were resuspended in 100 µl of sodium dodecyl sulfate buffer (2% SDS, 50 mM Tris pH 7.4). Protein concentrations were determined by Pierce BCA protein assay kit (Thermo Fisher Scientific, USA) according to the manufacturer's instructions. Samples were mixed with sample buffer (2% SDS, 50 mM Tris, 10% glycerol, 1% DTT, 0.1% bromophenol blue, pH 6.8). 15 µg of total tissue protein samples were electrophoresed into Biorad Criterion TGC Stain-Free 4–20% gels. Gels were transferred to PVDF membranes. PVDF membranes were washed in Tris-buffered saline with tween (TBST) (150 mM NaCl, 10 mM Tris, 0.075% Tween-20, pH 7.5) and incubated in 5% skim milk powder in TBST for 1 h at room temperature. Membranes were incubated with primary antibodies (amyloid-β, α-synuclein, NeuN, AQP4, GFAP, ADLH1L1, α-syntrophin or dystrophin) overnight at 4 °C and secondary antibody for 1 h at room temperature (see Suppl. Table 1 for antibodies concentration). In between each incubation step, membranes were washed in TBST. Membranes were visualized on an Amersham Imager 600 using Luminata Classico or Luminata Forte western blotting detection reagents. The density of the bands was measured using Amersham Imager 600 analysis software.

2.7. Histology analysis

Cresyl Violet staining was performed as previously described (Ong et al., 2018). For immunoperoxidase labelling and immunofluorescence, free-floating fixed sections corresponding to peri-infarct (Bregma 0.0 mm), and thalamus and hippocampus (Bregma −1.5 mm) were immunostained as described (Zhao et al., 2017). Images were acquired using Aperio AT2 (Leica, Germany) or Leica TCS SP8 confocal microscope. ImageJ (1.50, National Institutes of Health) and Matlab (R2015a, MathWorks) were used to estimate tissue loss and to analyse intensity and area coverage of immunolabeling. AQP4 polarity analysis were performed as previously described (Wang et al., 2012). In this case, each image was thresholded uniformly at two different levels: a high and a low stringency threshold (Supplementary Fig. 3(e)). The low stringency threshold defined the overall area of AQP4 immunoreactivity, whereas the high-stringency threshold defined the area of intense AQP4 immunoreactivity that in control mice is localized to perivascular end-feet of the astrocytes. The ratio of the low-stringency area to the high-stringency area was used to generate a value defined as "AQP4 polarity". The higher the AQP4 polarity, the greater proportion on immunoreactivity was restricted to perivascular regions, whereas the lower the proportion, the more evenly distributed immunoreactivity was between the perivascular end-feet and the soma. (For detailed image analysis see Supplementary material).

2.8. Statistics

All data were expressed as mean ± SD and were analysed using GraphPad Prism v7.02. The primary outcome measurement was differences between sham and stroke. Data from ELISA, tissue loss, western blotting, immunohistochemistry and immunofluorescence labelling were analysed using 2-tailed *t*-test. VD task (10 sessions temporal analysis) and motor test were analysed using 2-way ANOVA, followed by Sidak multiple comparisons. A p value $< .05$ was considered statistically significant.

3. Results

3.1. Cortical stroke induces cognitive impairment and motor deficits

Three days after the induction of the stroke targeting the motor and sensory cortex, the cognitive performance of the mice were assessed using a mouse touchscreen platform for VD task during 10 consecutive days (Fig. 1A). The first cohort of mice (sham $n = 10$, stroke $n = 11$) was evaluated using two images with a low similarity index ('marble-fan' pair). We observed a significant time effect ($F_{(4,\ 76)} = 14.35$, $p < .0001$) but no significant differences in the % correct trials in stroked mice compared with sham (Fig. 1B). The second cohort (sham $n = 10$, stroke $n = 11$) were subjected to the same VD task, however images were substituted for a high similarity index pair ('ovals-rectangles' pair). We found a significant decrease in % correct trials in stroked mice compared to sham ($F_{(1,\ 19)} = 23.74$, $p = .0001$) and a significant time effect ($F_{(4,\ 76)} = 7.81, p < .0001$). In addition, post hoc analysis indicated a significant decrease in rate of % correct trials at the fourth and fifth block of sessions in stroke mice compared to sham ($p = .0179$ and $p = .043$, respectively) (Fig. 1C). A range of metrics from the VD task were also collected for temporal analysis. There was no significant effect in the number of trials completed within 60 min nor in time to complete 30 trials, however, there was a significant increase in the number of total correction trials completed in stroke mice compared to sham ($p = .0426$) (Supplementary Fig. 2A, B and C).

The second cohort of mice were also tested for motor deficits one day before stroke and at 14 days post stroke. Locomotor asymmetry was evaluated using a cylinder task. Specifically, this evaluates the paw preference that mice exhibit for stabilising themselves while rearing within a cylinder. Data on asymmetry scores indicated that there were no significant differences in paw preference prior to stroke. However, at day 14 the stroke group exhibited a significantly stronger preference for using their unaffected paw (the paw not connected to the damaged hemisphere) relative to sham ($p < .0001$) (Fig. 2A).

3.2. Cortical stroke induces neuronal loss in the peri-infarct region and in SND sites

In order to assess the damage that the cortical stroke induced in the brain, we first estimated the tissue loss at bregma 0.0 mm level using Cresyl Violet staining. We observed that the stroke group had significantly increased levels of tissue loss relative to the sham group

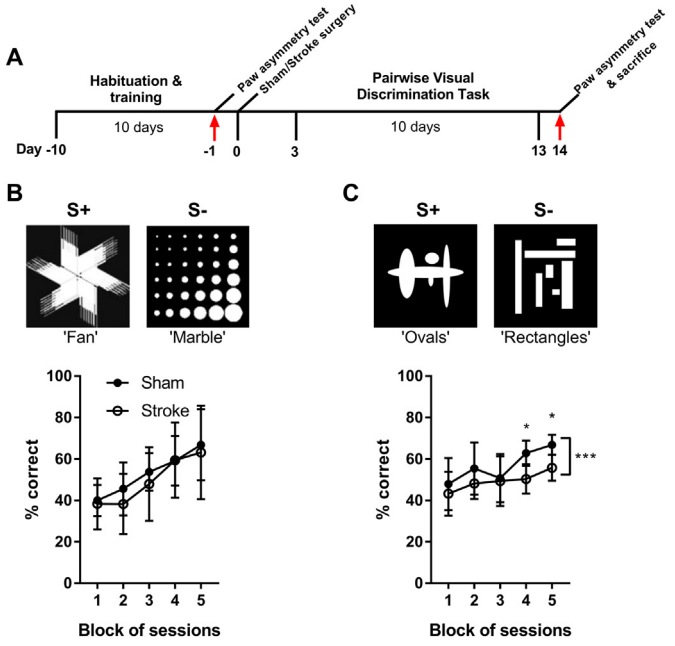

Fig. 1. Cortical stroke affects mice ability to discriminate between two images with a high similarity index, but not with low similarity index. (A) Experimental design timeline. (B) The first cohort of mice (sham $n = 10$, stroke $n = 11$) were subjected to VD task using two images with a low similarity index ('marble-fan' pair) (S+ correct and S- incorrect). No significant differences were found in the % correct responses between sham and stroke mice. (C) A second cohort (sham n = 10, stroke n = 11) was evaluated using a high similarity index pair ('ovals-rectangles' pair). We found a significant decrease in % correct responses in stroked mice compared to sham at fourth and fifth block of session. 1 block is the average of 2 sessions. Mean ± SD (two-way ANOVA and Sidak's multiple comparisons). *$p < .05$; ***$p < .001$.

($p < .0001$) (Fig. 2B).

To investigate whether neuronal loss occurs in the primary infarct area and in SND sites, we evaluated the protein levels of the mature neuronal marker (NeuN) in the peri-infarct, thalamus and hippocampus using Western blotting. Our analysis indicated a significant decrease in NeuN levels in the peri-infarct ($p = .0003$), thalamus ($p = .0023$) and hippocampus ($p = .0093$) (Fig. 2C).

We further confirmed the protein data using immunohistochemistry NeuN staining. We performed automated $NeuN^+$ cell count in peri-infarct and thalamus (Supplementary Fig. 3A). Data showed a significant decrease in $NeuN^+$ cells in both the peri-infarct ($p < .0001$) and thalamus ($p < .0001$) in stroke mice (Fig. 2D and E). In the hippocampus area, cell bodies are very densely packed making $NeuN^+$ cell count difficult. Instead, optical density was assessed using thresholding analyses (Supplementary Fig. 3B) in three different sub-regions of the hippocampus: CA1, CA3 and dentate gyrus (DG). We found a significant decrease in threshold material for NeuN only in the CA1 sub-region of stroke mice compared with sham ($p = .0138$) (Fig. 2D and E).

3.3. Cortical stroke leads to aggregation and accumulation of neurotoxic proteins

α-Synuclein: The supernatant and pellet fractions were analysed by western blotting for the levels of α-Syn. We evaluated the monomer (14 kDa), dimer (28 kDa) and trimer (42 kDa) levels. In the peri-infarct region, we found a significant increase in α-Syn dimer and trimer levels in both the supernatant and pellet fraction (supernatant dimer $p < .0001$; supernatant trimer $p = .0003$; pellet dimer $p = .0005$; pellet trimer $p = .0085$). In the thalamus, a significant reduction of monomer levels, and a corresponding significant increase in α-Syn trimer levels were observed in the supernatant fraction only (supernatant monomer $p = .0021$; supernatant trimer $p = .015$). No changes were detected in the pellet. In the hippocampus, we found no significant changes in the supernatant, however, we identified a significant increase in both monomer and trimer levels in the pellet fraction (pellet monomer $p = .0002$, pellet trimer $p = .0094$) (Fig. 3A and B).

To further validate the western blot results and understand the spatial distribution of α-Syn accumulation brain sections from different bregma regions corresponding with the peri-infarct region (Bregma 0.0 mm), thalamus and hippocampus (Bregma −1.5 mm) were analysed by immunohistochemistry using an antibody against α-Syn. Optical density of α-Syn staining was quantitatively assessed using the threshold analysis. Using ImageJ software, we identified that pixel intensity 120 detected genuine α-Syn immunoreactive material (Supplementary Fig. 3C). We found a significant increase in α-Syn accumulation in the peri-infarct ($p = .0198$), thalamus ($p = .0064$) and hippocampus (CA1 $p = .0037$, CA3 $p = .0004$, DG $p = .0004$) of stroked mice compared to sham (Fig. 3C). Pearson correlation analysis showed no significant correlation between the extent of α-Syn accumulation and cognitive performance within the stroke group ($r = -0.04335$, $P_{(Y=-0.01792*X+54.22)} = 0.8893$).

Amyloid-β: We investigated the Aβ aggregation status in both supernatant and pellet fractions. Specifically, we quantitated the pentamer (25 kDa), intermediate size oligomers (30 kDa), decamer (50 kDa) and dodecamer (56 kDa). In the peri-infarct area, we observed a significant increase in all of the supernatant and pellet oligomers in stroke mice compared with sham mice (supernatant pentamer $p = .00015$; supernatant intermediate size oligomer $p = .0032$; supernatant decamer $p < .0001$; supernatant dodecamer $p = .00096$; pellet pentamer $p = .0032$ and pellet decamer $p = .0008$). In the thalamus, we found a significant increase in the decamer both in the supernatant and pellet fraction (supernatant decamer $p < .0001$; pellet decamer $p = .0463$). In the hippocampus, we observed a significant increase in the intermediate size oligomers, decamer and dodecamer in the supernatant fraction (supernatant intermediate size oligomer $p = .0059$; supernatant decamer $p = .0033$; supernatant dodecamer $p = .00039$) and decamer in the pellet fraction (pellet decamer $p = .0003$) (Fig. 4A and B).

We also found a significant increase in Aβ immunolabeling at pixel intensity 120 (Supplementary Fig. 3C) in the peri-infarct ($p < .0001$), thalamus ($p = .0378$) and hippocampus (CA1 $p = .0003$; CA3 $p = .0077$; DG $p = .0085$) in stroke mice compared with sham (Fig. 4C). Pearson correlation analysis showed no significant correlation between the extent of Aβ accumulation and cognitive performance within the stroke group ($r = -0.1866$, $P_{(Y=-0.08497*X+57.46)} = 0.5828$).

3.4. Cortical stroke promotes astrogliosis and AQP4 dysregulation primarily in the peri-infarct region and thalamus

We next analysed the expression of astrocytic markers (ALDH1L1 and GFAP) in the peri-infarct region, thalamus and hippocampus at 14 days after stroke. Western blotting data revealed a significant increase in both ALDH1L1 and GFAP in the peri-infarct (ALDH1L1 $p = .0024$; GFAP $p = .0001$), thalamus (ALDH1L1 $p = .00031$; GFAP $p = .0001$) and hippocampus (ALDH1L1 $p = .0126$; GFAP $p = .0108$) in stroke mice compared to sham (Fig. 5A and B). We further confirmed the protein data using immunofluorescence, and found that stroke mice exhibited a significant increase in the GFAP-positive area in the peri-infarct region ($p < .0001$), thalamus ($p < .0001$) and in all the hippocampal sub-regions studied (CA1 $p < .0001$; CA3 $p < .0001$; DG $p = .0037$) (Fig. 6B, E and H).

Then, we analysed if stroke induced disturbances in the AQP4 water channel. Here, we observed a significant decreased in the AQP4 protein expression within the peri-infarct area ($p < .0001$) in stroke mice compared with sham. However, there were no significant changes of AQP4 protein levels in the thalamus or hippocampus (Fig. 5C). These

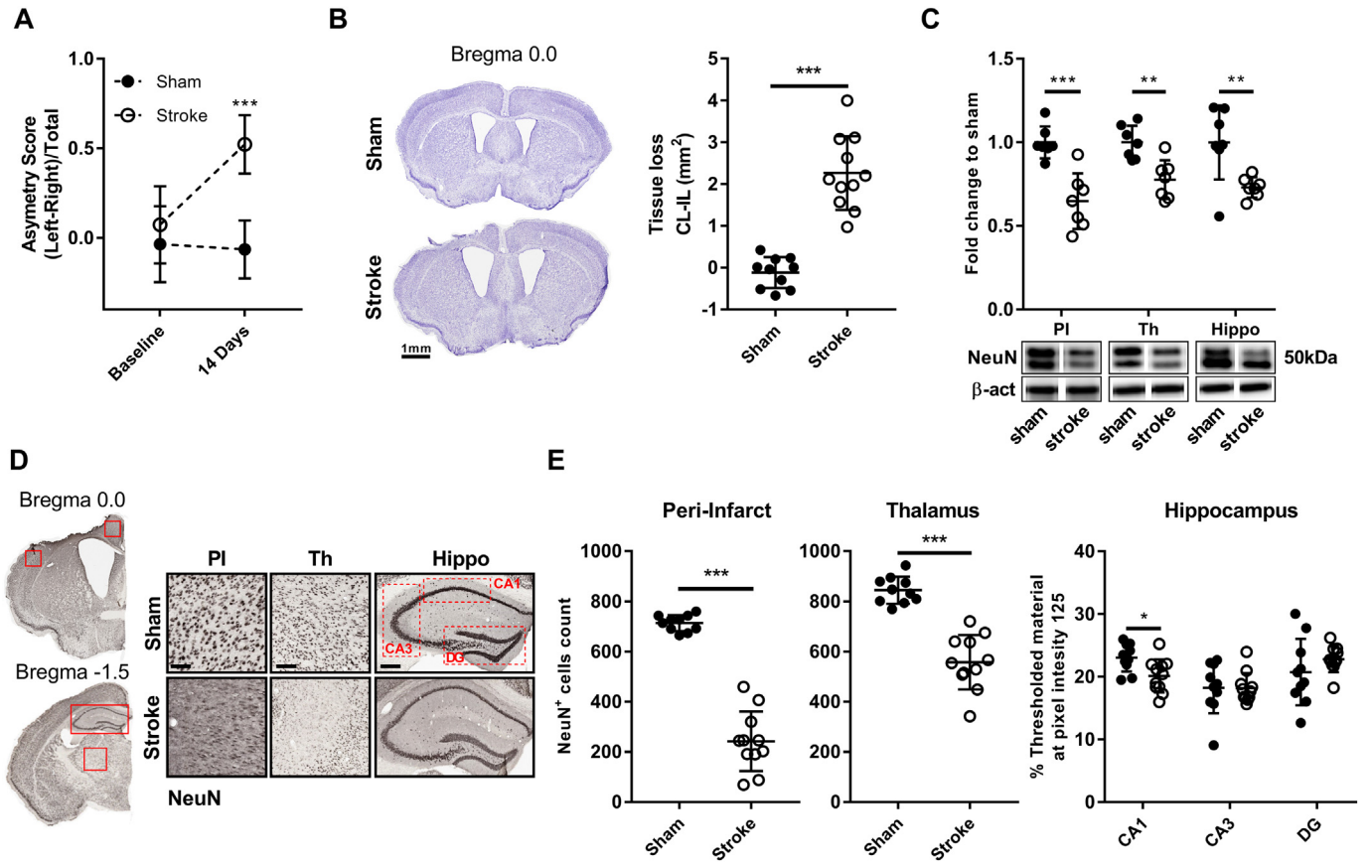

Fig. 2. Cortical stroke induces motor deficits and neuronal loss in the peri-infarct and in SND sites at 14 days. (A) Locomotor asymmetry was evaluated at baseline (one day before stroke induction) and at 14 days post-stroke using cylinder task (two-way ANOVA and Sidak's multiple comparisons). (B) Representative images of Cresyl violet staining at Bregma 0.0 mm. Tissue loss was calculated as contralateral (CL) hemisphere area − ipsilateral (IL) hemisphere area. (C) Representative western blot and quantification of NeuN protein levels within the peri-infarct (PI), thalamus (Th) and hippocampus (Hippo) for sham and stroke mice and loading control β-actin (β-act). (D). Representative immunohistochemistry labelling for NeuN. Left panel: red squares indicate the location of the peri-infarct, thalamus and hippocampus regions examined. Right panels: higher magnification images (PI scale bar = 100 μm, Th scale bar = 200 μm, Hippo scale bar = 300 μm). Dash area indicate the sub-regions of the hippocampus studied (CA1, CA3 and dentate gyrus (DG)). **(e)** Quantification of NeuN-positve cell within peri-infarct and thalamus. In the hippocampus area, optical density of NeuN staining was assessed using thresholding analyses. Mean ± SD (2-tailed *t*-test) * $p < .05$, ** $p < .01$ *** $p < .001$. (For interpretation of the references to colour in this figure legend, the reader is referred to the web version of this article.)

analyses provided us with information about the protein expression profile. However, it is necessary to investigate whether AQP4 remains polarised to perivascular astrocytic end-feet domains after stroke to ensure proper clearance and water distribution. Therefore, we carried out complementary immunofluorescence analyses co-labelling GFAP and AQP4. In sham animals, we observed that AQP4 is highly polarised to the end-feet of the astrocytes, however, after stroke we observed a clear mislocalisation of AQP4 (Fig. 6A, D and G). In addition to this qualitative analysis, we also measured AQP4 polarity as described previously (Wang et al., 2012). Higher AQP4 polarity values reflected expression levels of AQP4 in perivascular end-feet being greater than in surrounding tissue, while lower AQP4 polarity reflected a more even distribution between the perivascular end-feet and the soma. Our analysis revealed a loss of AQP4 polarity in the peri-infarct ($p = .002$) and thalamus ($p = .0103$) regions of mice receiving stroke compared with sham, but there were no significant changes in the hippocampus (Fig. 6C, F and I).

Finally, we investigated the protein expression profile of dystrophin and α-syntrophin, which are proteins of the dystrophin-associated complex responsible for maintaining AQP4 polarization to the end-feet of the astrocytes (Amiry-Moghaddam et al., 2004; Amiry-Moghaddam et al., 2003; Neely et al., 2001; Nicchia et al., 2008). Western blot analysis revealed a significant reduction in α-syntrophin within the peri-infarct ($p = .0054$) and a significant reduction in dystrophin within peri-infarct ($p < .0001$) and thalamus ($p = .0464$) territories in stroked mice compared to sham (Fig. 5D and E).

4. Discussion

We showed for the first time that photothrombotic vascular occlusion of the motor and somatosensory cortex has a significant impact on the ability of the mice to learn how to discriminate between two different stimuli, as evaluated by a mouse touchscreen platform for VD task. Secondly, we observed a significant loss of neuronal cells post-stroke in the peri-infarct region and in SND sites, such as the thalamus and the CA1 sub-region of the hippocampus. We then focused our investigation on α-Syn and Aβ, which have previously been linked to cognitive impairment and neurodegenerative conditions. We identified an increase in the accumulation and aggregation of these neurotoxic proteins in the peri-infarct, thalamus and hippocampus. Finally, we demonstrated that stroke induces astrogliosis, AQP4 dysregulation and disturbances in the dystrophin-associated complex. Collectively, these results suggest that the cognitive impairment seen post-stroke might be due to an increased accumulation of neurotoxic proteins as a result of a failure of the clearance mechanisms to remove these waste products from the brain.

We utilised a photothrombotic stroke model in combination of a touchscreen platform to advance our understanding in post-stroke

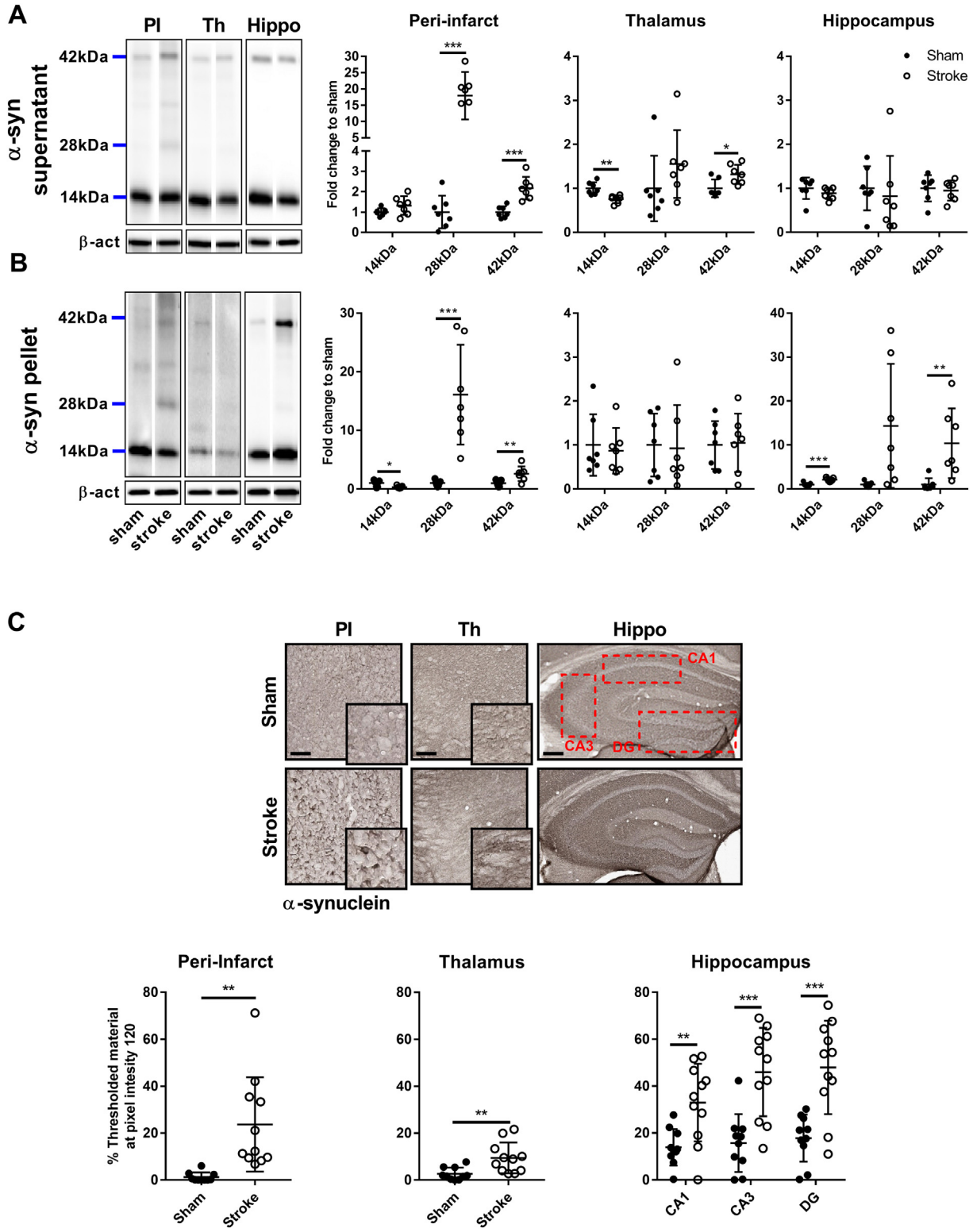

Fig. 3. Cortical stroke leads to aggregation and accumulation of α-Synuclein (α-Syn) at 14 days post-stroke. Representative western blot and quantification of α-Syn expression profile within the peri-infarct (PI), thalamus (Th) and hippocampus (hippo) in the supernatant (A) and pellet (B) fraction. Our analyses focused on the monomer (14 kDa), dimer (28 kDa) and trimer (42 kDa). (C) Representative images of α-Syn immunostaining and high magnification detail (PI scale bar = 100 μm, Th scale bar = 200 μm, Hippo scale bar = 300 μm). Dash area indicate the sub-regions of the hippocampus studied (CA1, CA3 and dentate gyrus (DG)). Quantification of material thresholded at the pixel intensity 120 shows an increased deposition of α-Syn. Mean ± SD (2-tailed *t*-test). * $p < .05$, ** $p < .01$ *** $p < .001$.

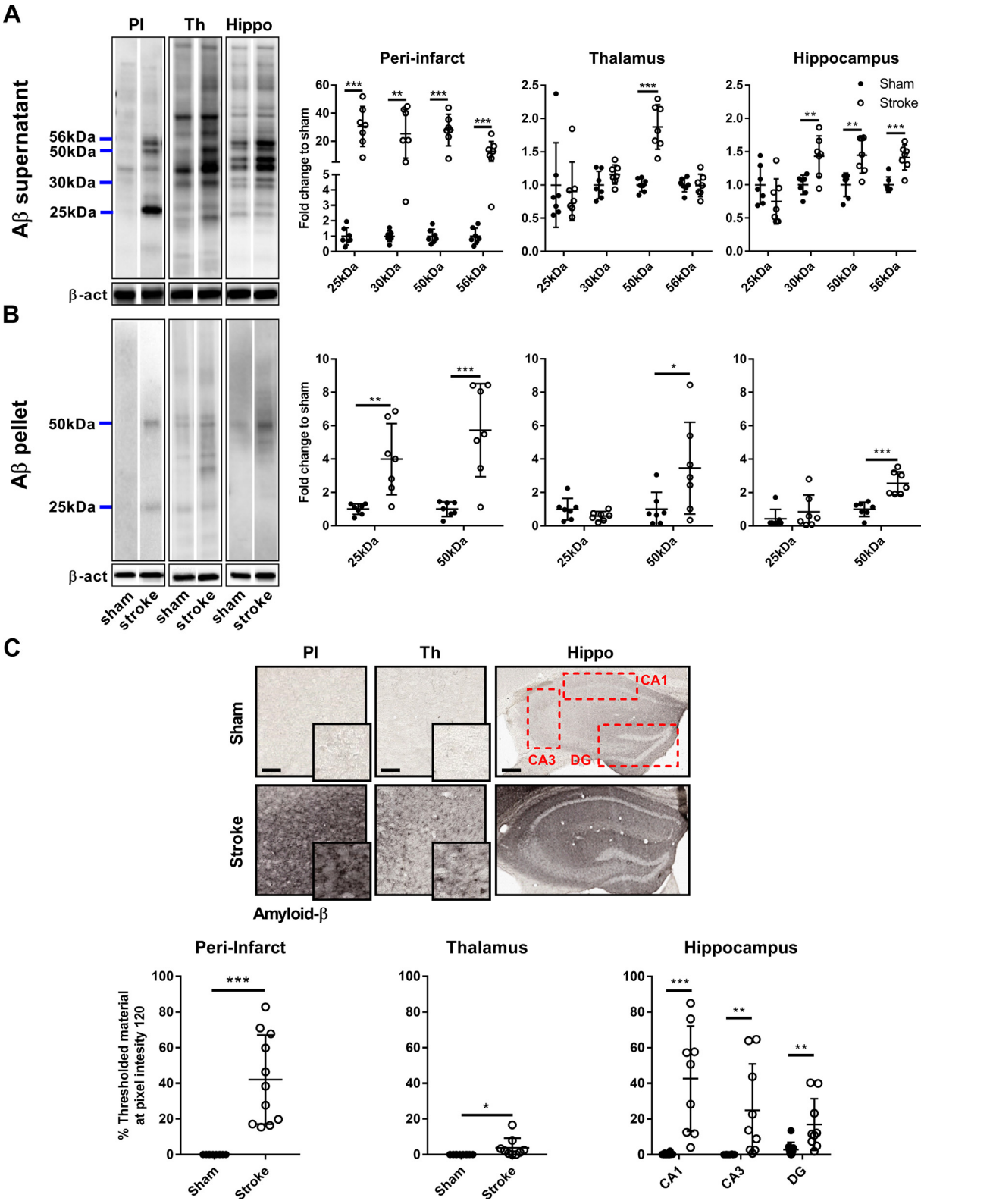

Fig. 4. Cortical stroke leads to aggregation and accumulation of Amyloid-β (Aβ) at 14 days post-stroke. Representative western blot and quantification of Aβ expression profile within the peri-infarct (PI), thalamus (Th) and hippocampus (hippo) in the supernatant (A) and pellet (B) fraction. Our analyses focused on different molecular weight oligomers (25 kDa, 30 kDa, 50 kDa and 56 kDa). Our results showed a significant increase in different molecular weight oligomers and accumulation after stroke. We observed a consistent increased of the 50 kDa oligomer. (C) Representative images of Aβ immunostaining and high magnification detail (PI scale bar = 100 μm, Th scale bar = 200 μm, Hippo scale bar = 300 μm). Dash area indicate the sub-regions of the hippocampus studied (CA1, CA3 and dentate gyrus (DG)). Quantification of material thresholded at the pixel intensity 120 shows an increased deposition of Aβ. Mean ± SD (2-tailed *t*-test). * $p < .05$, ** $p < .01$ *** $p < .001$.

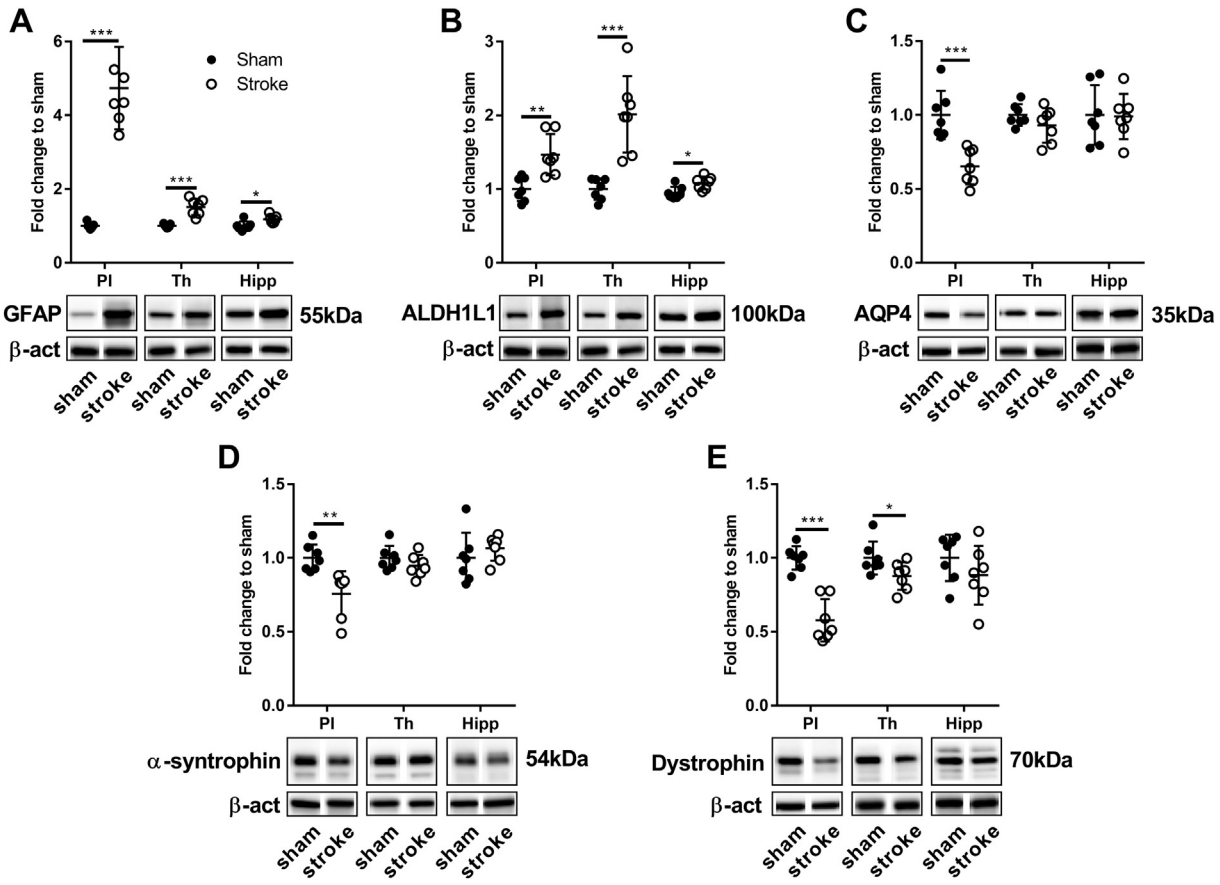

Fig. 5. Cortical stroke promote astrogliosis, AQP4 dysregulation and disturbance in the proteins of the dystrophin-associated complex at 14 days. Representative western blot and quantification of astrocytic markers GFAP (A) and ALDH1L1 (B) within the peri-infarct (PI), thalamus (Th) and hippocampus (hippo). (C) Representative western blot and quantification of aquaporin 4 (AQP4) water channel. Representative western blot and quantification of α-syntrophin (D) and dystrophin (E) within the peri-infarct (PI), thalamus (Th) and hippocampus (hippo). Mean ± SD (2-tailed *t*-test). * $p < .05$, ** $p < .01$ *** $p < .001$.

cognitive impairment (Bussey et al., 2008). Classically, the Morris water maze has been the gold-standard test for assessing cognition, however, in the context of stroke recovery, this task is cofounded by motor impairment and a ceiling effect that reduce its sensitivity in assessing cognition (Balkaya et al., 2018; Morris, 1984; Shepherd et al., 2016). Further, this task could be perceived as a stressful condition, a factor that negatively affect cognition (Ong et al., 2017b; Zhao et al., 2017). To assess these deficits, we chose a more sensitive and translationally relevant platform, utilising touchscreen testing (Balkaya et al., 2018; Horner et al., 2013; Schaar et al., 2010; Shepherd et al., 2016). Specifically, we focused on the VD task, in which mice must learn to consistently respond to one of two visual stimuli to be rewarded. One of the critical variables that we wished to determine was the relative difficulty of the stimuli presented. To address this, we considered two image sets (low similarity and high similarity). When the low similarity pair was tested ('marble-fan' pair, typically used in previous studies (Morton et al., 2006; Romberg et al., 2013)), no differences in cognitive performance were observed between stroked and sham mice. We then considered the performance of mice using the high similarity pair ('oval-rectangles' pair). In this case, we observed a significant decrease in the % of correct trials between 10 and 14 days post-stroke in stroke mice compared to sham. Together, this data identified that the sensitivity of the VD task to unmask cognitive deficits varies as a function of the similarity of the image sets.

One important factor to consider in interpreting the VD performance data is the dependence of the task on motor function. Clearly, the touchscreen tasks require intact motor function such that subjects are able to traverse the testing chamber, respond to the screen, and collect a reward (Horner et al., 2013). As such, one possible interpretation of the data we have reported is that they reflect a motor impairment of the mice rather than a cognitive deficit. In favour of this explanation, we did observe that stroked mice exhibited a stronger preference for using their unaffected paw during a spontaneous rearing task, which is consistent with prior findings (Zalewska et al., 2018; Zhao et al., 2017). However, despite this data, we could find no evidence of a motor deficit impacting the VD task as neither the number of trials completed within 60 min nor the time taken to complete 30 trials were statistically significant between the sham and stroke groups. This result indicates that any motor deficits present did not meaningfully affect the assessment of cognitive performance. This is consistent with a previous observation from our group that stroke does not alter the distance covered using the open field task (Zalewska et al., 2018). Given these results, we suggest that stroke affects the ability of the mice to discriminate between two different stimuli with a high similarity index, and these cognitive deficits are independent of the motor impairment caused by the photothrombotic stroke.

We then examined tissue loss and neuronal loss in order to assess the damage that the cortical stroke induced in the brain. Stroke mice exhibited a significant increase in tissue loss around the infarct site, which is consistent with previous observations (Zalewska et al., 2017; Zhao et al., 2017). The tissue loss after stroke includes loss of neurons (Karl et al., 2010), and neuronal loss is expected in the primary infarct site and in SND sites (Baumgartner et al., 2018; Tamura et al., 1991; Zhang et al., 2012b). Here, we identified a significant decrease in NeuN-positive cells in the peri-infarct region, thalamus and also the CA1 subregion of the hippocampus. The decrease in the number of neurons in the hippocampus is an important finding that could explain the cognitive impairment seen after stroke and reinforces the idea that stroke

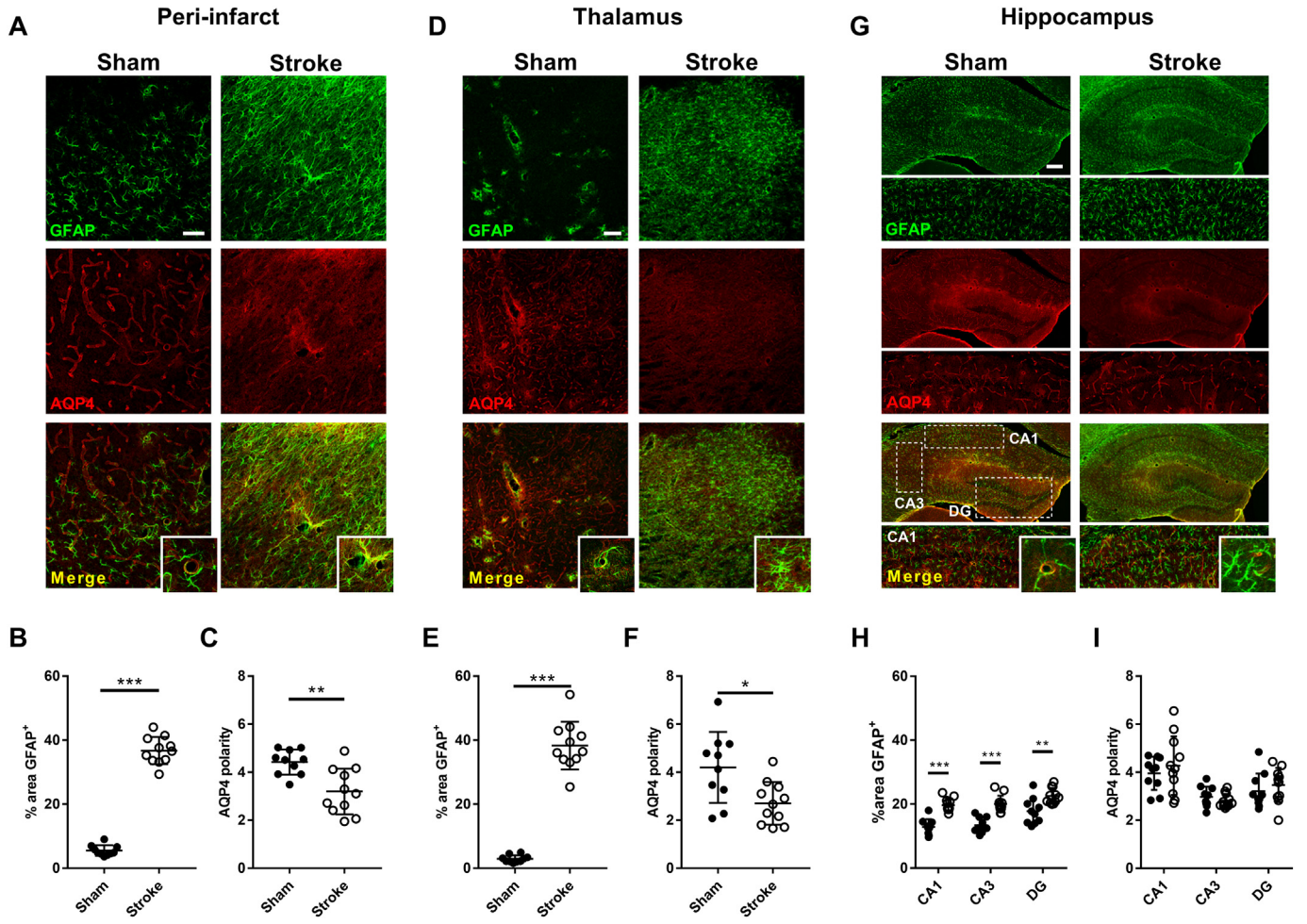

Fig. 6. Cortical stroke promote astrogliosis and AQP4 dysregulation. Representative immunofluorescence images of peri-infarct (A), thalamus (D) and hippocampus (G) co-labelled with GFAP (green) and AQP4 (red) (PI scale bar = 50 μm, Th scale bar = 100 μm, Hippo scale bar = 200 μm). White dash area indicate the sub-regions of the hippocampus studied (CA1, CA3 and dentate gyrus (DG)). Quantification of reactive astrogliosis (% area of GFAP$^+$) in the peri-infarct (B), thalamus (E) and hippocampus (H). (C, F and I) Changes in AQP4 polarity were also measured in these same regions. In sham animals, AQP4 is highly polarised to perivascular end-feet of astrocytes. We observed a partial loss of the AQP4 polarity in the peri-infarct and thalamus area but not in the hippocampus at 14 days post-stroke. Mean ± SD (2-tailed *t*-test). * $p < .05$, ** $p < .01$ *** $p < .001$. (For interpretation of the references to colour in this figure legend, the reader is referred to the web version of this article.)

induces alterations in remote regions that are functionally connected to the primary ischemic area (Wang et al., 2004; Xie et al., 2011). A recent study by Baumgartner et al. (2018) also supports this idea by providing in vivo evidence that a sensorimotor stroke induces a dysfunction in the hippocampal-thalamic network.

In terms of further considering the mechanisms involved in this neuronal loss and cognitive impairment, we investigated whether stroke altered the aggregation and accumulation of two neurotoxic proteins. First, we studied α-Syn, which is a natively soluble unfolded protein that undergoes spontaneous aggregation under different environmental conditions and plays a central role in chronic neurodegenerative diseases (Breydo et al., 2012; Stoica et al., 2012). In the context of stroke, previous studies have shown that an ischemic insult in adult mice lead to increased levels of α-Syn in the cortex (Kim et al., 2016; Unal-Cevik et al., 2011) and a knockdown or knockout of α-Syn significantly decreased infarct volume and promoted better motor recovery (Kim et al., 2016). To investigate the aggregation of α-Syn, we analysed both supernatant and pellet protein fractions using western blotting. We observed an increase in α-Syn oligomerization in all regions of neuronal loss. We further confirmed this observation using immunohistochemistry. Oligomeric forms of α-Syn have been previously described to be crucial structures underlying neuronal death and cognitive deficits in neurodegenerative diseases through several mechanisms such as inflammation, oxidative stress and autophagy (Dias et al., 2013; Pacheco et al., 2012). Interestingly, all these mechanism have been found to mediate post-stroke neuronal death and therefore it is reasonable to hypothesise that α-Syn might also play an important role in cognitive impairment after stroke.

A second protein extensively implicated in neurodegeneration is Aβ (Haass and Selkoe, 2007; Lesne et al., 2006; Lesne et al., 2013). Here, we studied how stroke alters the Aβ aggregation status in multiple regions of the brain. Previous studies have mainly focused on the Aβ deposition in the peri-infarct region (Garcia-Alloza et al., 2011) and the thalamus (Ong et al., 2017a; van Groen et al., 2005; Zhao et al., 2018). Our results showed a significant increased oligomerization in these two regions and in the hippocampus after stroke. Interestingly, we observed a consistent increase of the 50 kDa oligomer within the supernatant and pellet fraction of all the brain regions. Several studies have indicated that these Aβ oligomers, rather than the monomers or insoluble fibrils, may be responsible for the cellular pathology and cognitive decline in Alzheimer's disease (Lesne et al., 2006; Lesne et al., 2013). We also investigated whether the plasma levels of Aβ40 and Aβ42 could be used as a predictor for cognitive impairment after stroke; however, we did not observe significant differences (Supplementary Fig. 4A and B). This is consistent with previous studies where blood levels of Aβ were only increased in the first 3 days after stroke, and decreased to baseline

levels by day 7 (Liu et al., 2015b) and day 30 post-stroke (Howe et al., 2018).

Taking our findings on α-Syn and Aβ together, we suggest that that the aggregation and accumulation of neurotoxic protein after stroke may be more widespread than expected, involving regions far from the primary infarct. The association of neuronal loss and protein aggregation suggest that greater levels of α-Syn and Aβ accumulation seen in the brain, especially in the hippocampus, might be responsible for neuronal death and cognitive impairment seen after stroke. In studies of neurodegenerative diseases, Wilson et al. (Wilson et al., 2017) investigated the impact of the early Aβ accumulation on visual discrimination dysfunction in an Alzheimer's disease (AD) rat model. They observed an intraneuronal accumulation of Aβ soluble oligomers occurring in the hippocampus and neocortex. This accumulation of Aβ altered synaptic plasticity through persistent inhibition of long-term potentiation in the CA1 area of the hippocampus which, in turn, severely impaired the visual discrimination learning. This similar effect might be also happening in the context of stroke.

There are several possible mechanisms to explain this increase in neurotoxic protein load: an increase in the rate of production, a decrease in the rate of degradation, or impaired clearance. Here, we focused particularly on the role of the clearance mechanisms in the accumulation of these neurotoxic proteins. It is well documented that the astrocytes have end-feet processes which wrap around the cerebral blood vessels, with a highly localized channel protein, AQP4 (Iliff et al., 2012; Mestre et al., 2018). AQP4 allows the bidirectional movement of water, which allows the exchange of the CSF with the ISF of the parenchyma, and forms a gradient for the removal of interstitial solutes (Verkman and Mitra, 2000). Reactive astrogliosis has been associated with the loss of perivascular AQP4 polarization in several brain injury models (Iliff et al., 2014; Ren et al., 2013; Wang et al., 2012). Therefore, we investigated whether the reactive astrogliosis and AQP4 dysfunction were present in the primary infarct area and in sites of SND. In this study, we found that widespread astrogliosis was evident throughout all the regions studied in the brains of stroke mice, consistent with our previous study (Patience et al., 2015). Our analysis also showed decreased levels of the AQP4 protein in the peri-infarct region of stroke mice but no significant differences were found in the thalamus or hippocampus. It should be noted that the assessment of AQP4 protein levels alone cannot conclusively determine whether AQP4 remains polarised to perivascular astrocytic end-feet. We therefore performed immunofluorescence analysis co-labelling GFAP and AQP4. AQP4 polarization was assessed by image analysis as previously described (Wang et al., 2012). In the peri-infarct and thalamus territories, AQP4 polarity was significantly reduced 14 days after stroke, however, no significant differences were found in the hippocampus. The disturbances in AQP4 reported here are consistent with previous studies in stroke and different neuropathological conditions (Ren et al., 2013; Wang et al., 2012; Zhao et al., 2018) and supports our hypothesis that loss of perivascular AQP4 polarization might impair the clearance of neurotoxic proteins away from the brain environment. AQP4 could represent a potential therapeutic target to improve neurotoxic protein clearance. Previous pre-clinical studies have shown that the accumulation of Aβ after stroke could be ameliorated using different therapeutic interventions targeting the Aβ production or clearance pathways (Sarajarvi et al., 2012; Zhang et al., 2012a; Zhang et al., 2011). This reduction has also been linked to an improvement in functional outcomes.

The investigation of AQP4 related proteins, such as the dystrophin-associated complex proteins, showed significantly reduced expression of both α-syntrophin and dystrophin in the peri-infarct area, and also significantly reduced dystrophin expression in the thalamus. These proteins position AQP4 to the perivascular astrocytic end-feet membrane allowing the bidirectional movement of water and solutes (Amiry-Moghaddam et al., 2004; Neely et al., 2001; Nicchia et al., 2008). Previous studies have reported that α-syntrophin knockout (Amiry-Moghaddam et al., 2003; Neely et al., 2001) and dystrophin-null (Vajda et al., 2002) mice exhibited a dramatic reduction of AQP4 in astroglial end-feet surrounding blood vessels and interfered with the transport of water across the brain-blood interface. Our results were consistent with the immunofluorescence analyses that showed a reduction in AQP4 polarity exclusively in the peri-infract and thalamus, indicating a possible role of α-syntrophin and dystrophin in the AQP4 polarization disturbances and therefore the solute clearance after stroke. One important consideration is that we did not directly quantify CSF clearance, and future functional tests using in vivo/advanced imaging techniques are warranted to confirm the role of AQP4 in neurotoxic proteins clearance after stroke.

Our results have some limitations. Firstly, this is a cross-sectional study at 14 days post-stroke. We cannot conclusively answer which of these processes has occurred first or identify any underlying cause. In addition to the observed neuronal loss, accumulation of neurotoxic proteins and dysregulation of astrocytic AQP4, well documented mechanisms such as trans-synaptic apoptosis are most likely involved in the cascade of processes resulting in SND. This warrants further investigation. Critically, this study is an important first step in building an understanding of the post-stroke mechanisms affecting cognitive impairment. To gain a further understanding of related mechanisms, a longitudinal investigation would be necessary. Secondly, we have only examined discrimination learning and therefore other cognitive domains such as executive function, working memory and attention should be investigated in future studies. In addition, it would certainly be worthwhile to assess whether these cognitive deficits persist long-term.

In conclusion, this study demonstrates that the induction of stroke in the motor and sensory cortex induces cognitive deficits, specifically the ability to discriminate between stimuli with a high degree of similarity. This provides further evidence that cognitive impairment induced by stroke could be due to a series of secondary mechanisms, leading to the death of neuronal cells at the thalamus and the CA1 subregion of the hippocampus. Our findings of increased α-Syn and Aβ in the peri-infarct region, thalamus and hippocampus post-stroke suggest that these neurotoxic proteins are likely to contribute to post-stroke cognitive impairment. Finally, we also demonstrated that disturbances in the AQP4 polarization might play an important role in the failure of removing these neurotoxic proteins from the brain environment. Therapeutic strategies to improve brain waste clearance may be promising approaches to prevent post-stroke cognitive impairment.

Acknowledgements

This study was supported by Hunter Medical Research Institute (HMRI 896), Faculty of Health and Medicine Pilot Grant, Priority Research Centre for Stroke and Brain Injury Research Support Grant, Mary Costello Alzheimer's Pilot Grant and The University of Newcastle, Australia. LKO and SSB also acknowledge support from Research Advantage for ECR Higher Degree by Research (HDR) Scholarship and Greaves Family Postgraduate Scholarships in Medical Research (HMRI 1054).

Declaration of conflicting interests

The author(s) declared no potential conflicts of interest with respect to the research, authorship, and/or publication of this article.

Appendix A. Supplementary data

Supplementary data to this article can be found online at https://doi.org/10.1016/j.expneurol.2019.05.001.

References

Aho, L., Jolkkonen, J., Alafuzoff, I., 2006. Beta-amyloid aggregation in human brains with cerebrovascular lesions. Stroke 37, 2940–2945. https://doi.org/10.1161/01.Str.0000248777.44128.93.

Amiry-Moghaddam, M., Otsuka, T., Hurn, P.D., Traystman, R.J., Haug, F.M., Froehner, S.C., Adams, M.E., Neely, J.D., Agre, P., Ottersen, O.P., Bhardwaj, A., 2003. An alpha-syntrophin-dependent pool of AQP4 in astroglial end-feet confers bidirectional water flow between blood and brain. Proc. Natl. Acad. Sci. U. S. A. 100, 2106–2111. https://doi.org/10.1073/pnas.0437946100.

Amiry-Moghaddam, M., Frydenlund, D.S., Ottersen, O.P., 2004. Anchoring of aquaporin-4 in brain: molecular mechanisms and implications for the physiology and pathophysiology of water transport. Neuroscience 129, 999–1010. https://doi.org/10.1016/j.neuroscience.2004.08.049.

Arbel-Ornath, M., Hudry, E., Eikermann-Haerter, K., Hou, S., Gregory, J.L., Zhao, L., Betensky, R.A., Frosch, M.P., Greenberg, S.M., Bacskai, B.J., 2013. Interstitial fluid drainage is impaired in ischemic stroke and Alzheimer's disease mouse models. Acta Neuropathol. 126, 353–364. https://doi.org/10.1007/s00401-013-1145-2.

Balkaya, M.G., Trueman, R.C., Boltze, J., Corbett, D., Jolkkonen, J., 2018. Behavioral outcome measures to improve experimental stroke research. Behav. Brain Res. 352, 161–171. https://doi.org/10.1016/j.bbr.2017.07.039.

Baumgartner, P., El Amki, M., Bracko, O., Luft, A.R., Wegener, S., 2018. Sensorimotor stroke alters hippocampo-thalamic network activity. Sci. Rep. 8 (15770). https://doi.org/10.1038/s41598-018-34002-9.

Breydo, L., Wu, J.W., Uversky, V.N., 2012. Alpha-synuclein misfolding and Parkinson's disease. Biochim. Biophys. Acta 1822, 261–285. https://doi.org/10.1016/j.bbadis.2011.10.002.

Bussey, T.J., Padain, T.L., Skillings, E.A., Winters, B.D., Morton, A.J., Saksida, L.M., 2008. The touchscreen cognitive testing method for rodents: how to get the best out of your rat. Learn. Mem. (Cold Spring Harbor, N.Y.) 15, 516–523. https://doi.org/10.1101/lm.987808.

Corbett, D., Carmichael, S.T., Murphy, T.H., Jones, T.A., Schwab, M.E., Jolkkonen, J., Clarkson, A.N., Dancause, N., Wieloch, T., Johansen-Berg, H., Nilsson, M., McCullough, L.D., Joy, M.T., 2017. Enhancing the alignment of the preclinical and clinical stroke recovery research pipeline: consensus-based core recommendations from the stroke recovery and rehabilitation roundtable translational working group. Int. J. Stroke 12, 462–471. https://doi.org/10.1177/1747493017711814.

Dias, V., Junn, E., Mouradian, M.M., 2013. The role of oxidative stress in Parkinson's disease. J. Park. Dis. 3, 461–491. https://doi.org/10.3233/jpd-130230.

Garcia-Alloza, M., Gregory, J., Kuchibhotla, K.V., Fine, S., Wei, Y., Ayata, C., Frosch, M.P., Greenberg, S.M., Bacskai, B.J., 2011. Cerebrovascular lesions induce transient beta-amyloid deposition. Brain 134, 3697–3707. https://doi.org/10.1093/brain/awr300.

Gottesman, R.F., Hillis, A.E., 2010. Predictors and assessment of cognitive dysfunction resulting from ischaemic stroke. Lancet Neurol. 9, 895–905. https://doi.org/10.1016/s1474-4422(10)70164-2.

Haass, C., Selkoe, D.J., 2007. Soluble protein oligomers in neurodegeneration: lessons from the Alzheimer's amyloid beta-peptide. Nat. Rev. Mol. Cell Biol. 8, 101–112. https://doi.org/10.1038/nrm2101.

Horner, A.E., Heath, C.J., Hvoslef-Eide, M., Kent, B.A., Kim, C.H., Nilsson, S.R., Alsio, J., Oomen, C.A., Holmes, A., Saksida, L.M., Bussey, T.J., 2013. The touchscreen operant platform for testing learning and memory in rats and mice. Nat. Protoc. 8, 1961–1984. https://doi.org/10.1038/nprot.2013.122.

Howe, M.D., Atadja, L.A., Furr, J.W., Maniskas, M.E., Zhu, L., McCullough, L.D., Urayama, A., 2018. Fibronectin induces the perivascular deposition of cerebrospinal fluid-derived amyloid-beta in aging and after stroke. Neurobiol. Aging 72, 1–13. https://doi.org/10.1016/j.neurobiolaging.2018.07.019.

Iizuka, H., Sakatani, K., Young, W., 1990. Neural damage in the rat thalamus after cortical infarcts. Stroke 21, 790–794.

Iliff, J.J., Wang, M., Liao, Y., Plogg, B.A., Peng, W., Gundersen, G.A., Benveniste, H., Vates, G.E., Deane, R., Goldman, S.A., Nagelhus, E.A., Nedergaard, M., 2012. A paravascular pathway facilitates CSF flow through the brain parenchyma and the clearance of interstitial solutes, including amyloid beta. Sci. Transl. Med. 4, 147ra111. https://doi.org/10.1126/scitranslmed.3003748.

Iliff, J.J., Chen, M.J., Plog, B.A., Zeppenfeld, D.M., Soltero, M., Yang, L., Singh, I., Deane, R., Nedergaard, M., 2014. Impairment of glymphatic pathway function promotes tau pathology after traumatic brain injury. J. Neurosci. 34, 16180–16193. https://doi.org/10.1523/jneurosci.3020-14.2014.

Karl, J.M., Alaverdashvili, M., Cross, A.R., Whishaw, I.Q., 2010. Thinning, movement, and volume loss of residual cortical tissue occurs after stroke in the adult rat as identified by histological and magnetic resonance imaging analysis. Neuroscience 170, 123–137. https://doi.org/10.1016/j.neuroscience.2010.06.054.

Kim, T., Mehta, S.L., Kaimal, B., Lyons, K., Dempsey, R.J., Vemuganti, R., 2016. Poststroke induction of alpha-Synuclein mediates ischemic brain damage. J. Neurosci. 36, 7055–7065. https://doi.org/10.1523/jneurosci.1241-16.2016.

Kluge, M.G., Abdolhoseini, M., Zalewska, K., Ong, L.K., Johnson, S.J., Nilsson, M., Walker, F.R., 2018. Spatiotemporal analysis of impaired microglia process movement at sites of secondary neurodegeneration post-stroke. J. Cereb. Blood Flow Metab. https://doi.org/10.1177/0271678x18797346. 271678x18797346.

Kuzma, E., Lourida, I., Moore, S.F., Levine, D.A., Ukoumunne, O.C., Llewellyn, D.J., 2018. Stroke and dementia risk: a systematic review and meta-analysis. Alzheimers Dement. 14, 1416–1426. https://doi.org/10.1016/j.jalz.2018.06.3061.

Lesne, S., Koh, M.T., Kotilinek, L., Kayed, R., Glabe, C.G., Yang, A., Gallagher, M., Ashe, K.H., 2006. A specific amyloid-beta protein assembly in the brain impairs memory. Nature 440, 352–357. https://doi.org/10.1038/nature04533.

Lesne, S.E., Sherman, M.A., Grant, M., Kuskowski, M., Schneider, J.A., Bennett, D.A., Ashe, K.H., 2013. Brain amyloid-beta oligomers in ageing and Alzheimer's disease. Brain 136, 1383–1398. https://doi.org/10.1093/brain/awt062.

Levine, D.A., Galecki, A.T., Langa, K.M., Unverzagt, F.W., Kabeto, M.U., Giordani, B., Wadley, V.G., 2015. Trajectory of cognitive decline after incident stroke. Jama 314, 41–51. https://doi.org/10.1001/jama.2015.6968.

Liu, W., Wong, A., Au, L., Yang, J., Wang, Z., Leung, E.Y., Chen, S., Ho, C.L., Mok, V.C., 2015a. Influence of amyloid-beta on cognitive decline after stroke/transient ischemic attack: three-year longitudinal study. Stroke 46, 3074–3080. https://doi.org/10.1161/strokeaha.115.010449.

Liu, Y.H., Cao, H.Y., Wang, Y.R., Jiao, S.S., Bu, X.L., Zeng, F., Wang, Q.H., Li, J., Deng, J., Zhou, H.D., Wang, Y.J., 2015b. Serum Abeta is predictive for short-term neurological deficits after acute ischemic stroke. Neurotox. Res. 27, 292–299. https://doi.org/10.1007/s12640-015-9518-z.

Makinen, S., van Groen, T., Clarke, J., Thornell, A., Corbett, D., Hiltunen, M., Soininen, H., Jolkkonen, J., 2008. Coaccumulation of calcium and beta-amyloid in the thalamus after transient middle cerebral artery occlusion in rats. J. Cereb. Blood Metab. 28, 263–268. https://doi.org/10.1038/sj.jcbfm.9600529.

Mestre, H., Hablitz, L.M., Xavier, A.L., Feng, W., Zou, W., Pu, T., Monai, H., Murlidharan, G., Castellanos Rivera, R.M., Simon, M.J., Pike, M.M., Pla, V., Du, T., Kress, B.T., Wang, X., Plog, B.A., Thrane, A.S., Lundgaard, I., Abe, Y., Yasui, M., Thomas, J.H., Xiao, M., Hirase, H., Asokan, A., Iliff, J.J., Nedergaard, M., 2018. Aquaporin-4-dependent glymphatic solute transport in the rodent brain. Elife 7. https://doi.org/10.7554/eLife.40070.

Morris, R., 1984. Developments of a water-maze procedure for studying spatial learning in the rat. J. Neurosci. Methods 11, 47–60.

Morton, A.J., Skillings, E., Bussey, T.J., Saksida, L.M., 2006. Measuring cognitive deficits in disabled mice using an automated interactive touchscreen system. Nat. Methods 3, 767. https://doi.org/10.1038/nmeth1006-767.

Neely, J.D., Amiry-Moghaddam, M., Ottersen, O.P., Froehner, S.C., Agre, P., Adams, M.E., 2001. Syntrophin-dependent expression and localization of Aquaporin-4 water channel protein. Proc. Natl. Acad. Sci. U. S. A. 98, 14108–14113. https://doi.org/10.1073/pnas.241508198.

Nicchia, G.P., Rossi, A., Nudel, U., Svelto, M., Frigeri, A., 2008. Dystrophin-dependent and -independent AQP4 pools are expressed in the mouse brain. Glia 56, 869–876. https://doi.org/10.1002/glia.20661.

Ong, L.K., Walker, F.R., Nilsson, M., 2017a. Is stroke a neurodegenerative condition? A critical review of secondary Neurodegeneration and amyloid-beta accumulation after stroke. Aims Med. Sci. 4, 1–16.

Ong, L.K., Zhao, Z., Kluge, M., Walker, F.R., Nilsson, M., 2017b. Chronic stress exposure following photothrombotic stroke is associated with increased levels of amyloid beta accumulation and altered oligomerisation at sites of thalamic secondary neurodegeneration in mice. J. Cereb. Blood Flow Metab. 37, 1338–1348. https://doi.org/10.1177/0271678x16654920.

Ong, L.K., Chow, W.Z., TeBay, C., Kluge, M., Pietrogrande, G., Zalewska, K., Crock, P., Aberg, N.D., Bivard, A., Johnson, S.J., Walker, F.R., Nilsson, M., Isgaard, J., 2018. Growth hormone improves cognitive function after experimental stroke. Stroke 49, 1257–1266. https://doi.org/10.1161/strokeaha.117.020557.

Pacheco, C., Aguayo, L.G., Opazo, C., 2012. An extracellular mechanism that can explain the neurotoxic effects of alpha-synuclein aggregates in the brain. Front. Physiol. 3 (297). https://doi.org/10.3389/fphys.2012.00297.

Patience, M.J., Zouikr, I., Jones, K., Clarkson, A.N., Isgaard, J., Johnson, S.J., Walker, F.R., Nilsson, M., 2015. Photothrombotic stroke induces persistent ipsilateral and contralateral astrogliosis in key cognitive control nuclei. Neurochem. Res. 40, 362–371. https://doi.org/10.1007/s11064-014-1487-8.

Peng, W., Achariyar, T.M., Li, B., Liao, Y., Mestre, H., Hitomi, E., Regan, S., Kasper, T., Peng, S., Ding, F., Benveniste, H., Nedergaard, M., Deane, R., 2016. Suppression of glymphatic fluid transport in a mouse model of Alzheimer's disease. Neurobiol. Dis. 93, 215–225. https://doi.org/10.1016/j.nbd.2016.05.015.

Ren, Z., Iliff, J.J., Yang, L., Yang, J., Chen, X., Chen, M.J., Giese, R.N., Wang, B., Shi, X., Nedergaard, M., 2013. 'Hit & Run' model of closed-skull traumatic brain injury (TBI) reveals complex patterns of post-traumatic AQP4 dysregulation. J. Cereb. Blood Flow Metab. 33, 834–845. https://doi.org/10.1038/jcbfm.2013.30.

Romberg, C., Horner, A.E., Bussey, T.J., Saksida, L.M., 2013. A touch screen-automated cognitive test battery reveals impaired attention, memory abnormalities, and increased response inhibition in the TgCRND8 mouse model of Alzheimer's disease. Neurobiol. Aging 34, 731–744. https://doi.org/10.1016/j.neurobiolaging.2012.08.006.

Saczynski, J.S., Sigurdsson, S., Jonsdottir, M.K., Eiriksdottir, G., Jonsson, P.V., Garcia, M.E., Kjartansson, O., Lopez, O., van Buchem, M.A., Gudnason, V., Launer, L.J., 2009. Cerebral infarcts and cognitive performance: importance of location and number of infarcts. Stroke 40, 677–682. https://doi.org/10.1161/strokeaha.108.530212.

Sahathevan, R., Linden, T., Villemagne, V.L., Churilov, L., Ly, J.V., Rowe, C., Donnan, G., Brodtmann, A., 2016. Positron emission tomographic imaging in stroke: cross-sectional and follow-up assessment of amyloid in ischemic stroke. Stroke 47, 113–119. https://doi.org/10.1161/strokeaha.115.010528.

Sarajarvi, T., Lipsanen, A., Makinen, P., Peraniemi, S., Soininen, H., Haapasalo, A., Jolkkonen, J., Hiltunen, M., 2012. Bepridil decreases Abeta and calcium levels in the thalamus after middle cerebral artery occlusion in rats. J. Cell. Mol. Med. 16, 2754–2767. https://doi.org/10.1111/j.1582-4934.2012.01599.x.

Schaar, K.L., Brenneman, M.M., Savitz, S.I., 2010. Functional assessments in the rodent stroke model. Exp. Transl. Stroke Med. 2, 13. https://doi.org/10.1186/2040-7378-2-13.

Shepherd, A., Tyebji, S., Hannan, A.J., Burrows, E.L., 2016. Translational assays for assessment of cognition in rodent models of Alzheimer's disease and dementia. J. Mol. Neurosci. 60, 371–382. https://doi.org/10.1007/s12031-016-0837-1.

Stoica, G., Lungu, G., Bjorklund, N.L., Taglialatela, G., Zhang, X., Chiu, V., Hill, H.H.,

Schenk, J.O., Murray, I., 2012. Potential role of alpha-synuclein in neurodegeneration: studies in a rat animal model. J. Neurochem. 122, 812–822. https://doi.org/10.1111/j.1471-4159.2012.07805.x.

Sun, J.H., Tan, L., Yu, J.T., 2014. Post-stroke cognitive impairment: epidemiology, mechanisms and management. Ann. Transl. Med. 2, 80. https://doi.org/10.3978/j.issn.2305-5839.2014.08.05.

Tamura, A., Tahira, Y., Nagashima, H., Kirino, T., Gotoh, O., Hojo, S., Sano, K., 1991. Thalamic atrophy following cerebral infarction in the territory of the middle cerebral artery. Stroke 22, 615–618.

Unal-Cevik, I., Gursoy-Ozdemir, Y., Yemisci, M., Lule, S., Gurer, G., Can, A., Muller, V., Kahle, P.J., Dalkara, T., 2011. Alpha-synuclein aggregation induced by brief ischemia negatively impacts neuronal survival in vivo: a study in [A30P]alpha-synuclein transgenic mouse. J. Cereb. Blood Flow Metab. 31, 913–923. https://doi.org/10.1038/jcbfm.2010.170.

Uzdensky, A.B., 2018. Photothrombotic stroke as a model of ischemic stroke. Transl. Stroke Res. 9, 437–451. https://doi.org/10.1007/s12975-017-0593-8.

Vajda, Z., Pedersen, M., Fuchtbauer, E.M., Wertz, K., Stodkilde-Jorgensen, H., Sulyok, E., Doczi, T., Neely, J.D., Agre, P., Frokiaer, J., Nielsen, S., 2002. Delayed onset of brain edema and mislocalization of aquaporin-4 in dystrophin-null transgenic mice. Proc. Natl. Acad. Sci. U. S. A. 99, 13131–13136. https://doi.org/10.1073/pnas.192457099.

van Groen, T., Puurunen, K., Maki, H.M., Sivenius, J., Jolkkonen, J., 2005. Transformation of diffuse beta-amyloid precursor protein and beta-amyloid deposits to plaques in the thalamus after transient occlusion of the middle cerebral artery in rats. Stroke 36, 1551–1556. https://doi.org/10.1161/01.STR.0000169933.88903.cf.

Verkman, A.S., Mitra, A.K., 2000. Structure and function of aquaporin water channels. Am. J. Physiol. Renal Physiol. 278, F13–F28. https://doi.org/10.1152/ajprenal.2000.278.1.F13.

Wang, W., Redecker, C., Bidmon, H.J., Witte, O.W., 2004. Delayed neuronal death and damage of GDNF family receptors in CA1 following focal cerebral ischemia. Brain Res. 1023, 92–101. https://doi.org/10.1016/j.brainres.2004.07.034.

Wang, M., Iliff, J.J., Liao, Y., Chen, M.J., Shinseki, M.S., Venkataraman, A., Cheung, J., Wang, W., Nedergaard, M., 2012. Cognitive deficits and delayed neuronal loss in a mouse model of multiple microinfarcts. J. Neurosci. 32, 17948–17960. https://doi.org/10.1523/jneurosci.1860-12.2012.

Wang, M., Ding, F., Deng, S., Guo, X., Wang, W., Iliff, J.J., Nedergaard, M., 2017. Focal solute trapping and global glymphatic pathway impairment in a murine model of multiple microinfarcts. J. Neurosci. 37, 2870–2877. https://doi.org/10.1523/jneurosci.2112-16.2017.

Wilson, E.N., Abela, A.R., Do Carmo, S., Allard, S., Marks, A.R., Welikovitch, L.A., Ducatenzeiler, A., Chudasama, Y., Cuello, A.C., 2017. Intraneuronal Amyloid Beta Accumulation Disrupts Hippocampal CRTC1-Dependent Gene Expression and Cognitive Function in a Rat Model of Alzheimer Disease. Cereb. Cortex (New York, N.Y. : 1991) 27, 1501–1511. https://doi.org/10.1093/cercor/bhv332.

Xie, M., Yi, C., Luo, X., Xu, S., Yu, Z., Tang, Y., Zhu, W., Du, Y., Jia, L., Zhang, Q., Dong, Q., Zhu, W., Zhang, X., Bu, B., Wang, W., 2011. Glial gap junctional communication involvement in hippocampal damage after middle cerebral artery occlusion. Ann. Neurol. 70, 121–132. https://doi.org/10.1002/ana.22386.

Zalewska, K., Ong, L.K., Johnson, S.J., Nilsson, M., Walker, F.R., 2017. Oral administration of corticosterone at stress-like levels drives microglial but not vascular disturbances post-stroke. Neuroscience 352, 30–38. https://doi.org/10.1016/j.neuroscience.2017.03.005.

Zalewska, K., Pietrogrande, G., Ong, L.K., Abdolhoseini, M., Kluge, M., Johnson, S.J., Walker, F.R., Nilsson, M., 2018. Sustained administration of corticosterone at stress-like levels after stroke suppressed glial reactivity at sites of thalamic secondary neurodegeneration. Brain Behav. Immun. 69, 210–222. https://doi.org/10.1016/j.bbi.2017.11.014.

Zhang, Y., Xing, S., Zhang, J., Li, J., Li, C., Pei, Z., Zeng, J., 2011. Reduction of beta-amyloid deposits by gamma-secretase inhibitor is associated with the attenuation of secondary damage in the ipsilateral thalamus and sensory functional improvement after focal cortical infarction in hypertensive rats. J. Cereb. Blood Flow Metab. 31, 572–579. https://doi.org/10.1038/jcbfm.2010.127.

Zhang, J., Zhang, Y., Li, J., Xing, S., Li, C., Li, Y., Dang, C., Fan, Y., Yu, J., Pei, Z., Zeng, J., 2012a. Autophagosomes accumulation is associated with beta-amyloid deposits and secondary damage in the thalamus after focal cortical infarction in hypertensive rats. J. Neurochem. 120, 564–573. https://doi.org/10.1111/j.1471-4159.2011.07496.x.

Zhang, J., Zhang, Y., Xing, S., Liang, Z., Zeng, J., 2012b. Secondary neurodegeneration in remote regions after focal cerebral infarction: a new target for stroke management? Stroke 43, 1700–1705. https://doi.org/10.1161/strokeaha.111.632448.

Zhao, Z., Ong, L.K., Johnson, S., Nilsson, M., Walker, F.R., 2017. Chronic stress induced disruption of the peri-infarct neurovascular unit following experimentally induced photothrombotic stroke. J. Cereb. Blood Flow Metab. 37, 3709–3724. https://doi.org/10.1177/0271678x17696100.

Zhao, Z., Ong, L.K., Pietrogrande, G., Sanchez Bezanilla, S., Warren, K., Ilicic, M., Kluge, M.G., TeBay, C., Ottersen, O.P., Johnson, S.J., Nilsson, M., Walker, F.R., 2018. Low oxygen post conditioning improves stroke-induced cognitive impairment. bioRxiv. https://doi.org/10.1101/483453.